



# TGF- $\beta$ induces miR-182 to sustain NF- $\kappa$ B activation in glioma subsets

Libing Song,<sup>1</sup> Liping Liu,<sup>1</sup> Zhiqiang Wu,<sup>2,3</sup> Yun Li,<sup>3,4</sup> Zhe Ying,<sup>3,4</sup> Chuyong Lin,<sup>2,4</sup> Jueheng Wu,<sup>3,4</sup> Bo Hu,<sup>5</sup> Shi-Yuan Cheng,<sup>5</sup> Mengfeng Li,<sup>3,4</sup> and Jun Li<sup>2,4</sup>

<sup>1</sup>State Key Laboratory of Oncology in Southern China, Department of Experimental Research, Cancer Center,

<sup>2</sup>Department of Biochemistry, Zhongshan School of Medicine, <sup>3</sup>Key Laboratory of Tropical Disease Control, Ministry of Education, and

<sup>4</sup>Department of Microbiology, Zhongshan School of Medicine, Sun Yat-sen University, Guangzhou, China. <sup>5</sup>Department of Neurology, Brain Tumor Institute, Robert H. Lurie Comprehensive Cancer Center, Northwestern University Feinberg School of Medicine, Chicago, Illinois, USA.

**The strength and duration of NF- $\kappa$ B signaling are tightly controlled by multiple negative feedback mechanisms. However, in cancer cells, these feedback loops are overridden through unclear mechanisms to sustain oncogenic activation of NF- $\kappa$ B signaling. Previously, we demonstrated that overexpression of miR-30e\* directly represses I $\kappa$ B $\alpha$  expression and leads to hyperactivation of NF- $\kappa$ B. Here, we report that miR-182 was overexpressed in a different set of gliomas with relatively lower miR-30e\* expression and that miR-182 directly suppressed cylindromatosis (CYLD), an NF- $\kappa$ B negative regulator. This suppression of CYLD promoted ubiquitin conjugation of NF- $\kappa$ B signaling pathway components and induction of an aggressive phenotype of glioma cells both in vitro and in vivo. Furthermore, we found that TGF- $\beta$  induced miR-182 expression, leading to prolonged NF- $\kappa$ B activation. Importantly, the results of these experiments were consistent with an identified significant correlation between miR-182 levels with TGF- $\beta$  hyperactivation and activated NF- $\kappa$ B in a cohort of human glioma specimens. These findings uncover a plausible mechanism for sustained NF- $\kappa$ B activation in malignant gliomas and may suggest a new target for clinical intervention in human cancer.**

## Introduction

The NF- $\kappa$ B pathway, serving as a mechanistic link between inflammation and cancer development, is constitutively activated in various types of cancers (1–4). Over the last decade, ubiquitin (Ub) modification has emerged as an important regulatory mechanism for NF- $\kappa$ B signaling (5, 6). Notably, Ub conjugation is involved in nearly every step within the signaling cascades that lead to NF- $\kappa$ B activation. For example, during NF- $\kappa$ B activation by TNF- $\alpha$  or IL-1 $\beta$ , signaling intermediaries, such as TNF receptor-associated factors (TRAFs) and receptor interacting protein (RIP), are rapidly modified with K63-linked poly-Ub chains, facilitating recruitment and activation of TGF- $\beta$ -activated kinase 1 (TAK1) and I $\kappa$ B kinase (IKK) complexes (7–9). The activated IKK complex phosphorylates I $\kappa$ Bs, leading to assembly of K48-linked ubiquitination/degradation of I $\kappa$ B $\alpha$  and subsequent nuclear translocation and activation of NF- $\kappa$ B (10, 11). More recently, linear ubiquitination of NEMO and unanchored poly-Ub chains were also reported to be involved in NF- $\kappa$ B activation (12, 13).

On the other hand, NF- $\kappa$ B signaling is negatively controlled by Ub deconjugation mechanisms mediated by deubiquitinases, such as CYLD and A20 (14, 15). CYLD, a K63-specific deubiquitinase, has been demonstrated to switch off NF- $\kappa$ B signaling through specifically deubiquitinating K63-linked poly-Ub chains from multiple NF- $\kappa$ B signaling intermediaries, including TRAF2, TRAF6, RIP1, TAK1, NEMO, and BCL3 (16–18). A20, another suppressor of NF- $\kappa$ B, inhibits TNF- $\alpha$ -induced NF- $\kappa$ B activation by removing K63-linked poly-Ub chains from RIP1 and promotes addition of degradative K48-linked poly-Ub chains on RIP1 (19, 20). A20 can also deactivate the NF- $\kappa$ B signaling through dismantling K63-linked poly-Ub chains from TRAF2, TRAF6, and

NEMO (21). Moreover, several other factors, including TNIP1 and optineurin (OPTN), have been found to negatively regulate NF- $\kappa$ B signaling (22, 23).

The TGF- $\beta$ /Smad pathway is oncogenic in advanced tumors including high-grade gliomas, an aggressive and lethal human cancer (24). Elevated TGF- $\beta$  activity plays diverse roles in the progression of gliomas, such as promotion of cell proliferation, angiogenesis, invasiveness, and the self-renewal capacity of glioma-stem cells (25–28). Interestingly, although NF- $\kappa$ B activity is usually repressed by TGF- $\beta$  in normal cells, in cancer cells, NF- $\kappa$ B can be activated upon TGF- $\beta$  treatment, which suggests that NF- $\kappa$ B is an oncogenic mediator of TGF- $\beta$  signaling in tumors (29, 30). However, the functional cross-talk between TGF- $\beta$  and NF- $\kappa$ B signaling in cancer remains poorly understood.

Being able to coordinately regulate repertoires of target genes, microRNAs (miRNAs) can potentially modulate multiple steps of cancer development and progression (31, 32). We recently examined the alteration of miRNAs in human primary glioma tissues of various WHO tumor grades using microarray analysis and identified miR-182 as one of the most substantially overexpressed miRNAs in clinical gliomas (33). Herein, we report that miR-182 could be induced by TGF- $\beta$  and directly targeted and suppressed the 3'-untranslated regions (3'UTRs) of multiple genes that function as negative regulators of NF- $\kappa$ B, leading to NF- $\kappa$ B hyperactivation and aggressiveness of gliomas. These results identified a regulatory mechanism that renders NF- $\kappa$ B activation sustained in human gliomas, thereby supporting the functional and clinical significance of epigenetic events in cancer progression.

## Results

*Reduced CYLD levels in gliomas correlate with patient prognoses.* The CYLD deubiquitinase is a key negative regulator for NF- $\kappa$ B signaling (16–18), but its clinical significance and biological role in glioma

**Authorship note:** Libing Song and Liping Liu contributed equally to this work.

**Conflict of interest:** The authors have declared that no conflict of interest exists.

**Citation for this article:** *J Clin Invest.* 2012;122(10):3563–3578. doi:10.1172/JCI62339.

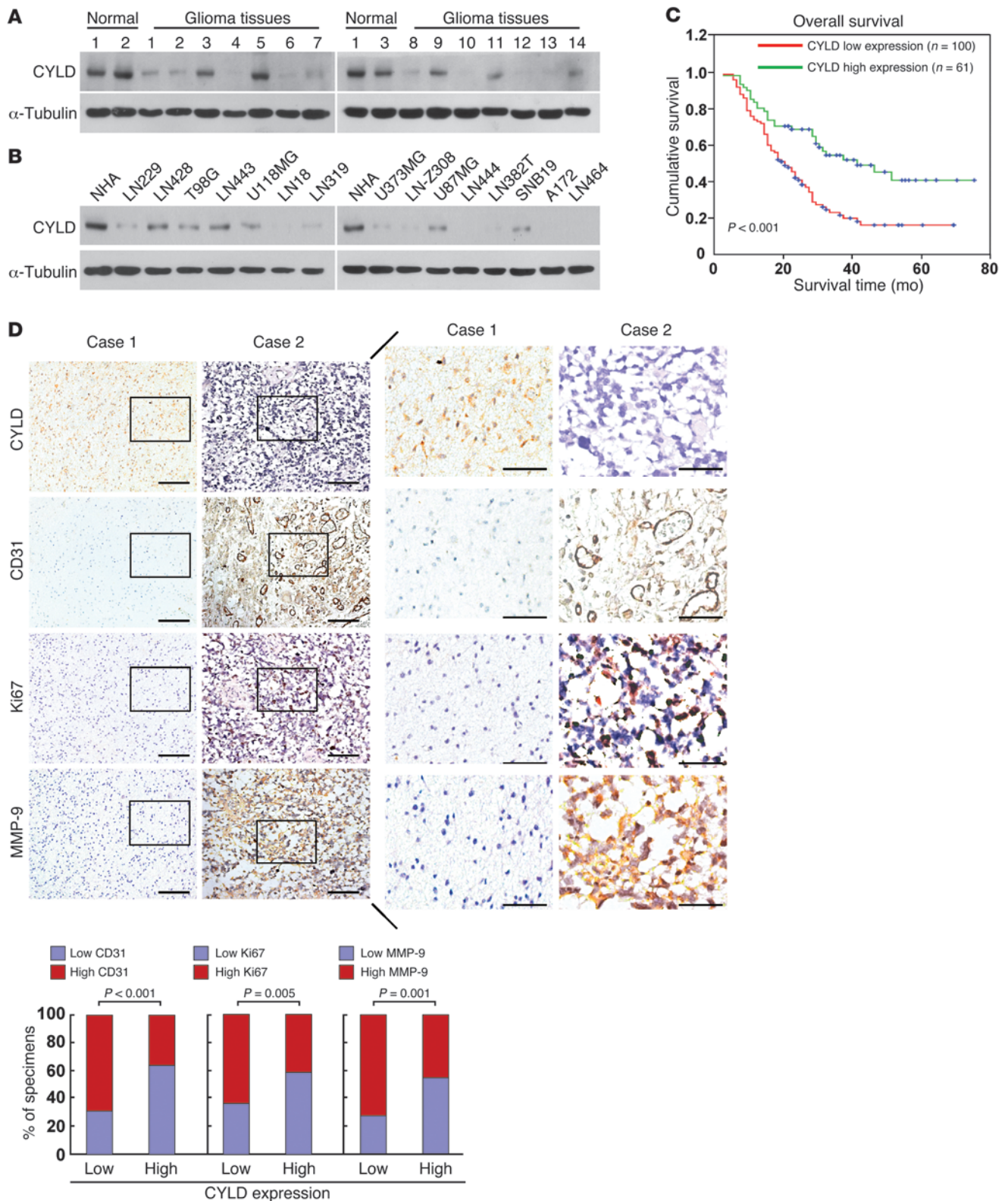


**Figure 1** Restoration of CYLD inhibits glioma tumorigenesis. (A and B) WB of CYLD in 3 normal brain tissues and 14 glioma tissues (A) and in NHAs and 15 individual glioma cell lines (B).  $\alpha$ -Tubulin was used as a loading control. (C) Kaplan-Meier analysis of CYLD expression in survival of patients with gliomas ( $P < 0.001$ , log-rank test;  $n = 161$ ). (D) CYLD expression was inversely associated with CD31, Ki67, and MMP-9 expression in 161 clinical glioma specimens. Shown are visualizations of 2 representative cases and percentages of samples showing low or high CYLD expression relative to CD31, Ki67, or MMP-9 levels. Scale bars: 100  $\mu$ m; 50  $\mu$ m (insets).

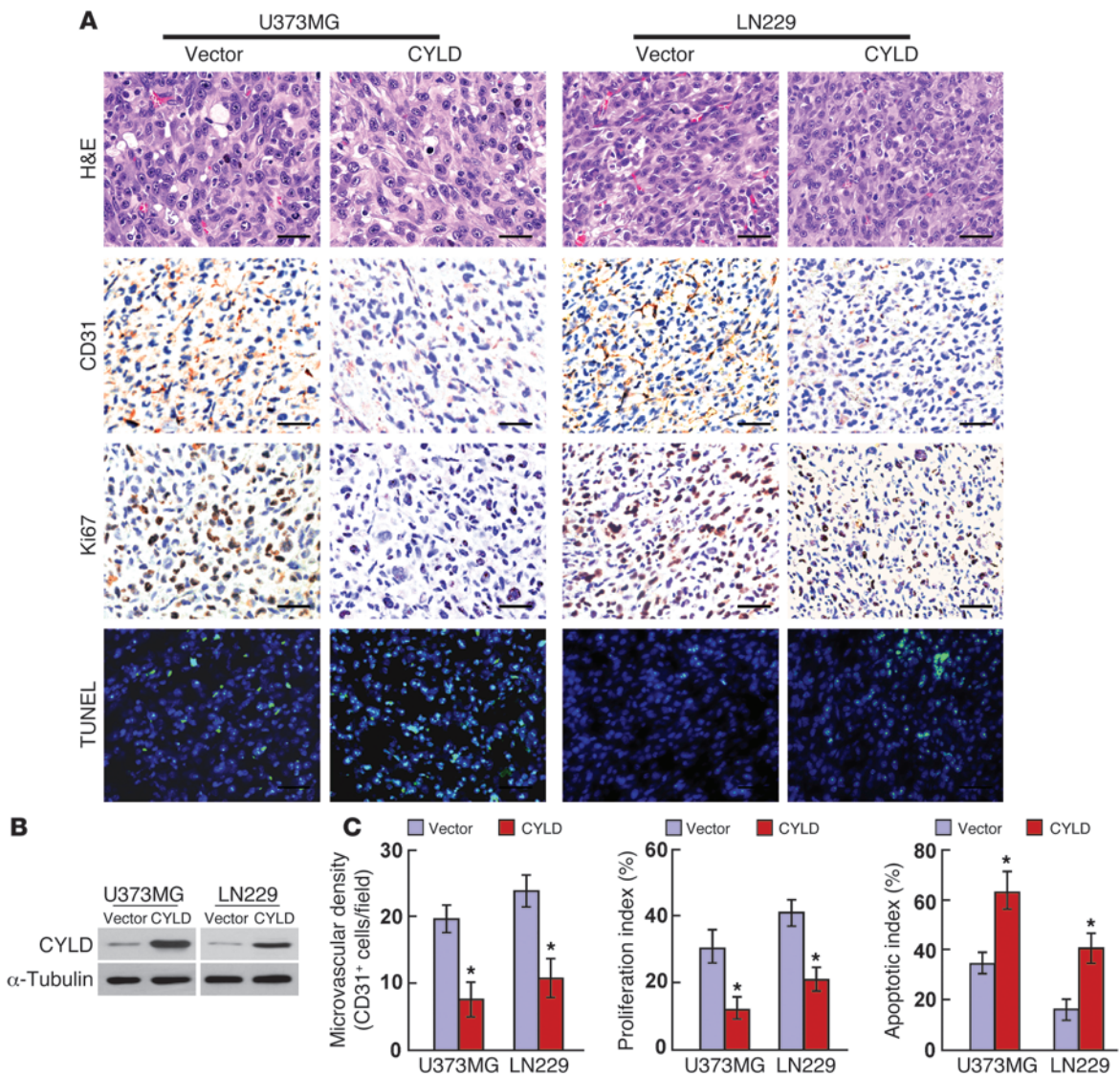


## Figure 2

Restoration of CYLD expression inhibits glioma growth and angiogenesis in vivo. Vector- or CYLD-transduced U373MG and LN229 glioma cells were stereotactically implanted into mouse brains. (A) Paraffin-embedded tumor sections were stained with H&E or with anti-CD31 or anti-Ki67 antibodies; apoptotic cells were visualized by TUNEL staining (green) and counterstained with DAPI (blue). (B) WB analysis of CYLD expression in vector- or CYLD-transduced U373MG and LN229 cells. (C) Quantification of microvascular density, proliferation index, and apoptotic index in glioma tumors. Error bars represent mean  $\pm$  SD from 3 independent experiments. Scale bars: 50  $\mu$ m. \* $P < 0.05$ .

mas remains unexplored. Using immunoblotting analysis, we found that CYLD expression was reduced in glioma tissues ( $n = 14$ ) and in all 15 glioma cell lines tested, compared with that in normal brain tissues ( $n = 3$ ) and in primary normal human astrocytes (NHAs) (Figure 1, A and B). Furthermore, statistical analysis revealed that CYLD levels inversely correlated with glioma WHO tumor grades ( $P < 0.001$ ) and were associated with shorter overall survival of patients with gliomas ( $P < 0.001$ ) ( $n = 161$ ; Figure 1C and Supplemental Tables 1–3; supplemental material available online with this article; doi:10.1172/JCI62339DS1). Additionally, we found that CYLD expression inversely correlated with levels of CD31 ( $P < 0.001$ ), Ki67 ( $P = 0.005$ ), and MMP-9 ( $P = 0.001$ ) (Figure 1D). All these data suggest a possible link between CYLD reduction and human glioma progression.

To investigate the biological effect of CYLD on gliomas, we modified U373MG and LN229 glioma cells to stably overexpress CYLD and stereotactically implanted them as well as control glioma cells into the brains of mice (Figure 2). Immunohistochemical (IHC) staining with an anti-CD31 antibody showed markedly decreased microvascular densities in CYLD-transduced versus control tumors (Figure 2A). The tumors formed by CYLD-transduced glioma cells also displayed lower cell proliferation indices and higher cell apoptosis (TUNEL-positive) compared with control tumors (Figure 2, B and C), which demonstrated that reconstitution of CYLD inhibited glioma growth and angiogenesis in the brain.

*miR-182 targets CYLD.* Consistent with published microarray data (NCBI/GEO/GSE4290;  $n = 180$ , specifically 23 nontumor and 157 tumor samples), we found no appreciable alteration of *CYLD*

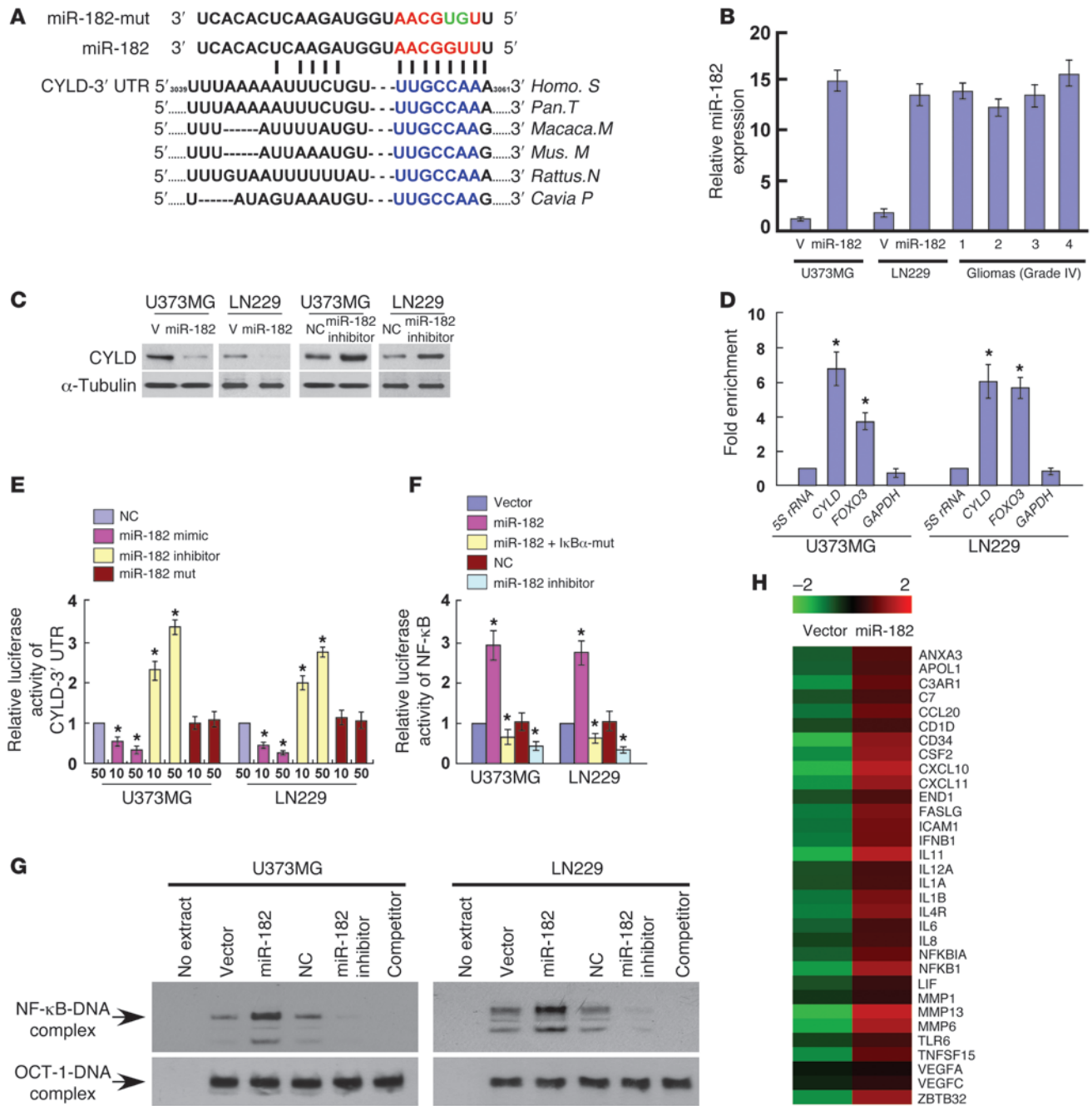


**Figure 3** miR-182 directly targets CYLD and activates NF- $\kappa$ B signaling. (A) Predicted miR-182 target sequence in CYLD-3'UTR and mutant containing 2 mutated nucleotides in the seed sequence of miR-182 (miR-182-mut). (B) Real-time PCR analysis of miR-182 expression in vector- (V) or miR-182-transduced cells and 4 WHO grade IV glioma samples. Transcript levels were normalized by *U6* expression. (C) WB of CYLD expression in vector- or miR-182-transduced cells, or the cells transfected with a negative control (NC) or a miR-182 inhibitor.  $\alpha$ -Tubulin was used as a loading control. (D) miRNP IP assay showed association of miR-182 with *CYLD*. *FOXO3* and *GAPDH* were used as positive and negative controls, respectively, and 5S rRNA was used as a control for overall expression levels. (E) Luciferase assay of cells separately transfected with a pGL3-CYLD-3'UTR reporter with increasing amounts (10 or 50 nM) of a miR-182 mimic, a miR-182 inhibitor, or a miR-182 mutant. (F) Luciferase reporter NF- $\kappa$ B activity. (G) EMSA of endogenous NF- $\kappa$ B activity markedly increased in miR-182-transduced glioma cells, but decreased in cells transfected with the miR-182 inhibitor. OCT-1 DNA-binding complex was used as a control. (H) GSEA showed an apparent overlap between NF- $\kappa$ B-dependent and miR-182-upregulated gene sets. Error bars represent mean  $\pm$  SD from 3 independent experiments. \**P* < 0.05.

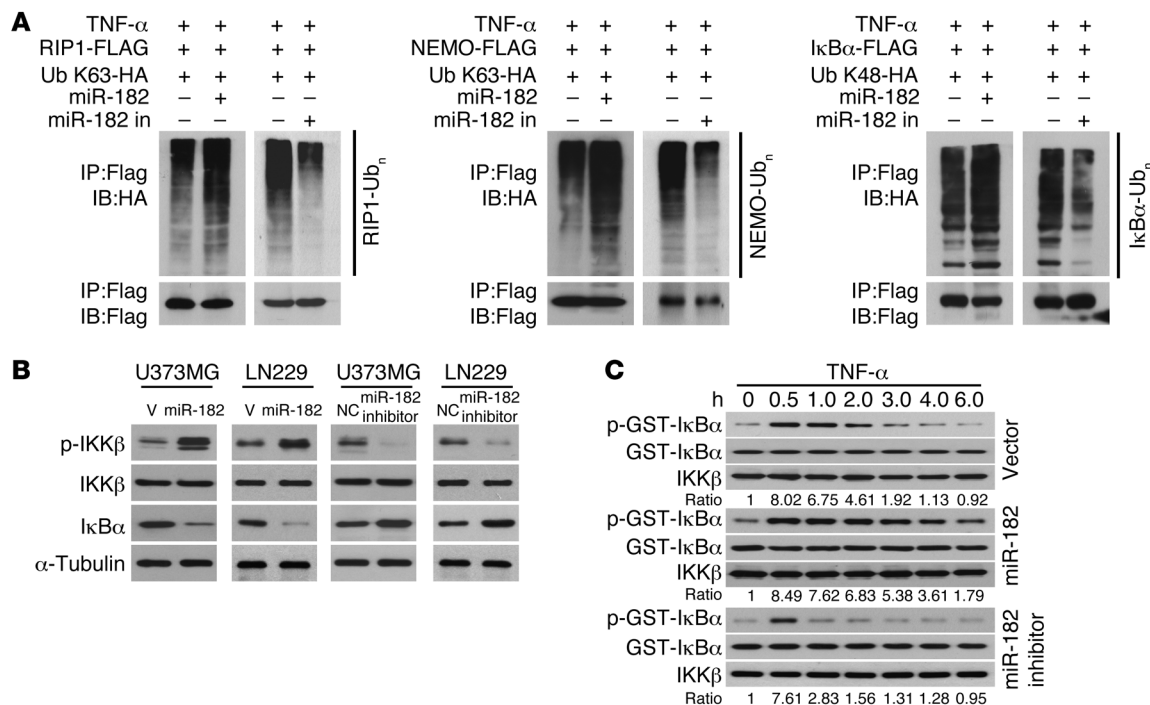


**Figure 4**

miR-182 sustains NF- $\kappa$ B activity. (A) WB of K63-linked poly-Ub of RIP1 and NEMO and K48-linked poly-Ub of I $\kappa$ B $\alpha$  in cells treated with 10 ng/ml TNF- $\alpha$ . in, inhibitor. (B) WB analysis of p-IKK $\beta$ , total IKK $\beta$ , and I $\kappa$ B $\alpha$  expression in cells treated with 10 ng/ml TNF- $\alpha$ . (C) In vitro kinase assay of vector- or miR-182-transduced cells, or miR-182 inhibitor-transfected cells treated with 10 ng/ml TNF- $\alpha$  for the indicated times (see Supplemental Methods). IKK $\beta$  was subjected to IP, and kinase activity was determined by phosphorylation of a recombinant GST-I $\kappa$ B $\alpha$  substrate using a phospho-specific I $\kappa$ B $\alpha$  antibody. Equal IP of IKK $\beta$  was shown. Error bars represent mean  $\pm$  SD from 3 independent experiments. \* $P$  < 0.05.

mRNA expression in glioma tissues compared with normal brains (Supplemental Figure 1, A and B), which suggests that reduction of CYLD protein in gliomas was not due to transcriptional inhibition. Interestingly, in analysis using publicly available algorithms (TargetScan), CYLD was predicted as a target of miR-182 (Figure 3A), one of the most substantially overexpressed miRNAs in clinical glioma specimens and glioma cell lines, including U373MG and LN229 cells (Figure 3B and ref. 33). To validate the effect of miR-182 on the inhibition of CYLD expression, U373MG and LN229 cells stably overexpressing miR-182 were established (Figure 3B). As shown in Figure 3C, CYLD expression decreased in miR-182-transduced cells, but increased in cells transfected with a miR-182 inhibitor. Nevertheless, the half-life of CYLD protein in miR-182-transduced cells was comparable to that in control cells (data not shown), which indicates that miR-182 did not induce CYLD protein degradation. Analyses by miRNP IP assay revealed a selective association of miR-182 with CYLD (Figure 3D). Notably, the inhibitory effect of miR-182 on the activity of luciferase reporter linked with the 3'UTR of CYLD (CYLD-3'UTR) was abolished by a miR-182 inhibitor. Moreover, a mutation introduced to miR-182 failed to reduce the luciferase activity, despite the presence of CYLD-3'UTR (Figure 3E). Collectively, these results established CYLD as a bona fide target of miR-182.

*miR-182 activates NF- $\kappa$ B signaling.* Since CYLD is a key negative regulator of NF- $\kappa$ B signaling (16–18), we investigated whether miR-182 is involved in NF- $\kappa$ B activation. Overexpression of miR-182 increased, while inhibition of miR-182 reduced, the luciferase activity of NF- $\kappa$ B reporter and expression of NF- $\kappa$ B target genes

(Figure 3F and Supplemental Figure 2A). In contrast, the stimulatory effect of miR-182 on NF- $\kappa$ B activity was reversed by transfection with an I $\kappa$ B $\alpha$  dominant-negative mutant (Figure 3F and Supplemental Figure 2B). Furthermore, EMSA showed that NF- $\kappa$ B activity was dramatically increased in miR-182-transduced cells, but decreased in miR-182-suppressed cells (Figure 3G). Analysis of the expression profiles of miR-182- and vector-transduced gliomas cells using the Gene Set Enrichment Analysis (GSEA) approach revealed significant overlap between miR-182-regulated genes and genes responsive to NF- $\kappa$ B activation (Figure 3H), further suggesting an important role of miR-182 in NF- $\kappa$ B activation.

*miR-182 sustains NF- $\kappa$ B activity.* Next, we examined the effect of miR-182 on the ubiquitination of molecules in the NF- $\kappa$ B signaling pathway. Upon TNF- $\alpha$  treatment, overexpressing miR-182 increased, while inhibiting miR-182 reduced, K63-linked poly-Ub levels of RIP1 and NEMO and the K48-linked poly-Ub level of I $\kappa$ B $\alpha$  (Figure 4A). Concordantly, miR-182 overexpression led to elevated phosphorylation of IKK $\beta$  and reduced I $\kappa$ B $\alpha$ , which was abrogated by the miR-182 inhibitor (Figure 4B). Importantly, in vitro kinase assay showed that endogenous IKK kinase activity was prolonged in miR-182-transduced cells upon TNF- $\alpha$  treatment. In contrast, IKK kinase activity after TNF- $\alpha$  treatment was rapidly decreased in miR-182-inhibited cells (Figure 4C). These results suggest that miR-182 promoted Ub conjugation in the NF- $\kappa$ B signaling and sustained NF- $\kappa$ B activity.

*miR-182 upregulation promotes glioma cell aggression in vitro and in vivo.* Consistent with our Gene Ontology enrichment analysis results (Figure 5A), we found that miR-182 overexpression mark-

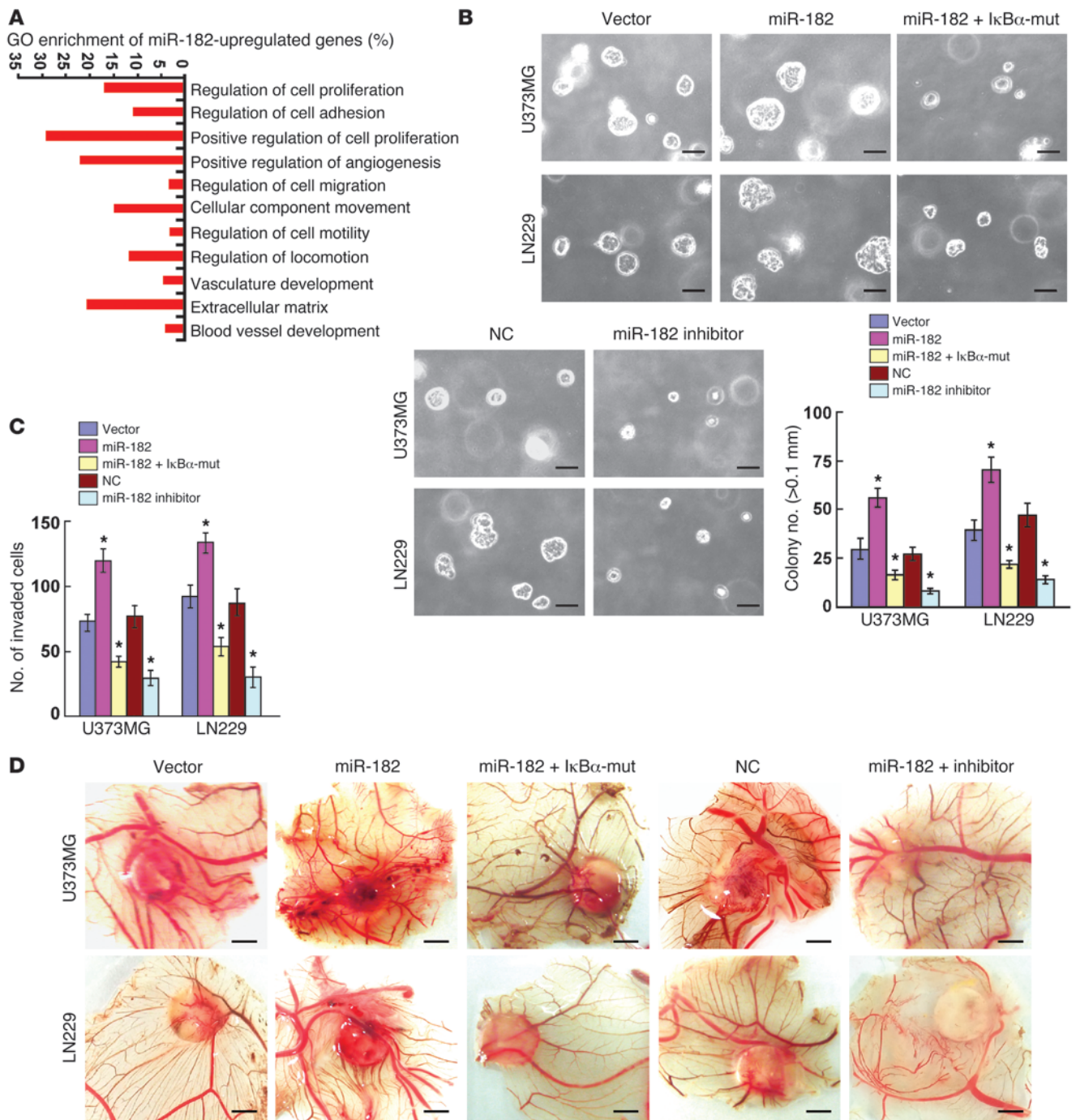


**Figure 5** miR-182 promotes aggressive phenotype of glioma cells in vitro. (A) Biofunctions of miR-182-regulated genes identified by microarray profiling in glioma cells. Enrichment of transcripts up- or downregulated ( $P < 0.05$ ) by miR-182 in duplicate experiments were determined by their Gene Ontology (GO) terms. (B) Representative micrographs and quantification of colonies determined by anchorage-independent growth assay. Scale bars: 100 μm. (C) Quantification of indicated invaded cells, analyzed by Transwell matrix penetration assay. (D) Representative images of chicken chorioallantoic membrane blood vessels stimulated with conditioned medium (see Supplemental Methods). Scale bars: 250 μm. Error bars represent mean ± SD from 3 independent experiments. \* $P < 0.05$ .

edly increased, while its suppression reduced, the anchorage-independent growth ability and invasiveness of both U373MG and LN229 cells (Figure 5, B and C). Meanwhile, miR-182 overexpression strongly provoked, whereas miR-182 inhibition abrogated,

the abilities of glioma cells to induce angiogenesis, as exhibited by the formation of second- and third-order vessels in chicken chorioallantoic membranes (Figure 5D). However, overexpressing the IκBα dominant-negative mutant markedly decreased the number

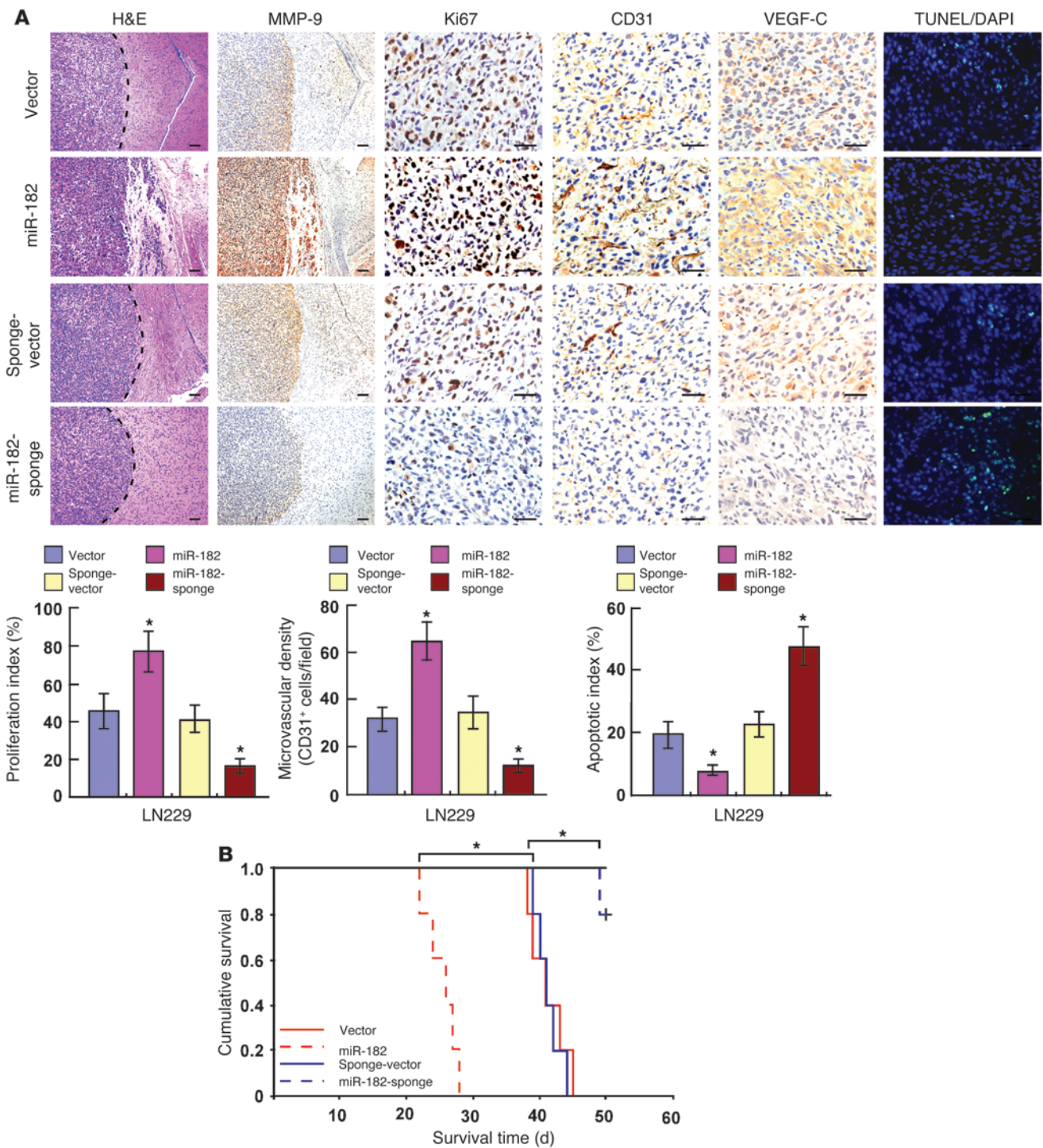


**Figure 6**

miR-182 promotes aggressive phenotype of glioma cells in vivo. (A) H&E and IHC staining showed that overexpression of miR-182 induced, while suppression of miR-182 inhibited, the aggressive phenotype of glioma cells in vivo — as indicated by CD31-, Ki67-, and TUNEL-positive cells — and invasion of glioma cells into surrounding brain tissues. Representative images of various brain sections were from 2 independent experiments with 5 mice per group with similar results. Scale bars: 100  $\mu$ m (H&E and MMP-9 IHC); 50  $\mu$ m (all others). (B) Kaplan-Meier survival of mice ( $n = 5$  per group) inoculated with the indicated cells. Error bars represent mean  $\pm$  SD from 3 independent experiments. \* $P < 0.05$ .

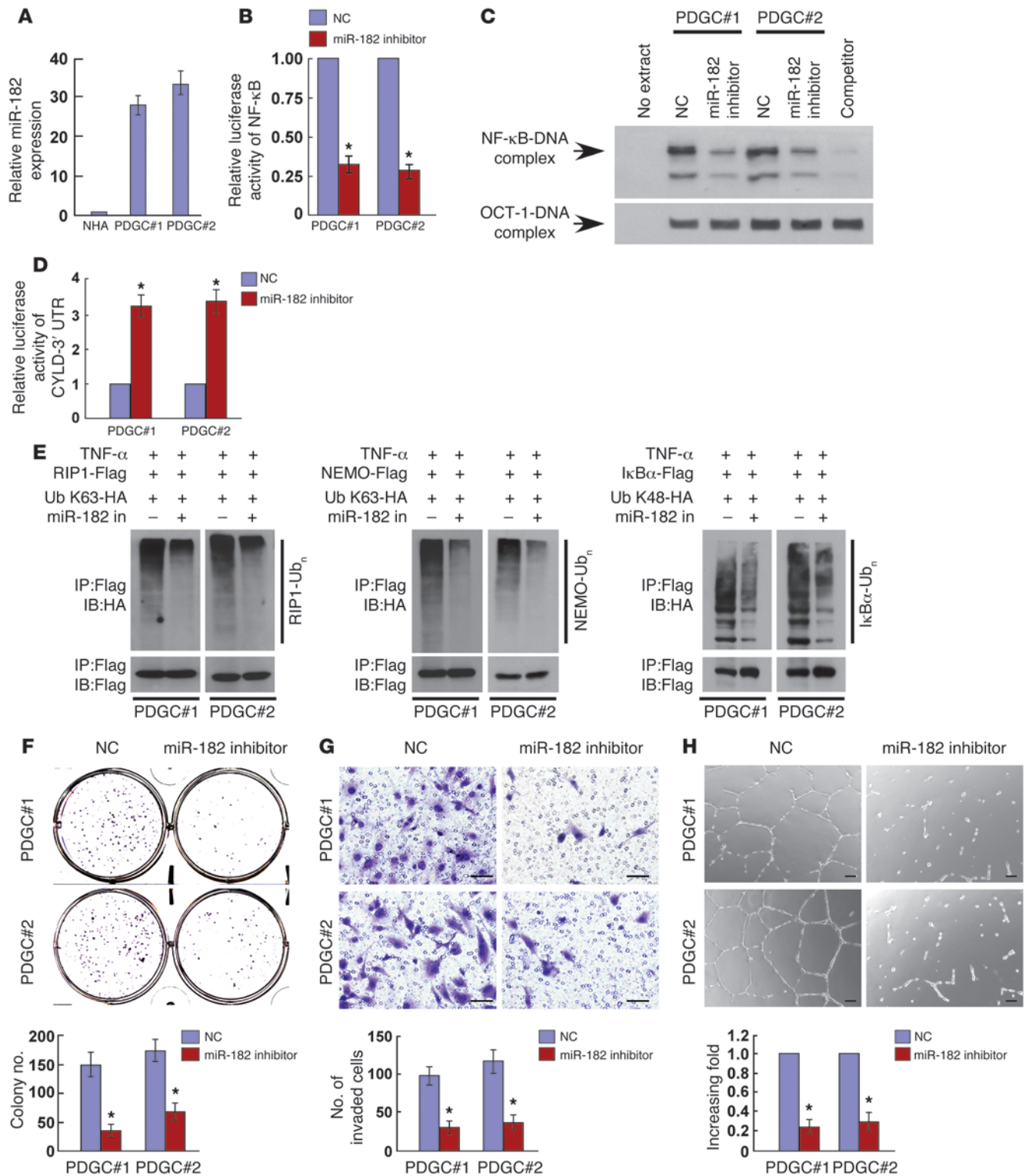




## Figure 7

Suppression of miR-182 inhibits NF- $\kappa$ B activity and malignant properties of PDGCs. (A) Real-time PCR analysis of miR-182 expression in NHAs and PDGCs derived from 2 separate glioma specimens. Transcript levels were normalized by *U6* expression. (B) NF- $\kappa$ B reporter activities in PDGCs derived from 2 separate glioma specimens transfected with a negative control or a miR-182 inhibitor. (C) EMSA of endogenous NF- $\kappa$ B activity showed a marked decrease in PDGCs transfected with the miR-182 inhibitor. OCT-1 DNA-binding complexes were used as a control. (D) Luciferase activity of CYLD-3'UTR in PDGCs transfected with negative control or the miR-182 inhibitor. (E) WB of K63-linked poly-Ub of RIP1 and NEMO and K48-linked poly-Ub of I $\kappa$ B $\alpha$  in negative control- or miR-182 inhibitor-transfected PDGCs treated with 10 ng/ml TNF- $\alpha$ . (F) Representative images and quantification of negative control- or miR-182 inhibitor-transfected PDGCs analyzed in a clonogenic assay (see Supplemental Methods). (G) Representative images and quantification of invaded cells analyzed using a Transwell matrix penetration assay. Scale bars: 50  $\mu$ m. (H) Representative images and quantification of HUVECs cultured on Matrigel-coated plates with conditioned medium from negative control- or miR-182 inhibitor-transfected PDGCs (see Supplemental Methods). Scale bars: 100  $\mu$ m. Error bars represent mean  $\pm$  SD from 3 independent experiments. \**P* < 0.05.

of colonies formed in soft agar by miR-182-transduced cells and reduced miR-182-induced invasiveness and angiogenesis (Figure 5, B–D), which suggests that functional NF- $\kappa$ B activation was critical for miR-182-mediated aggressiveness of glioma cells.

The biological role of miR-182 in promoting the aggressive phenotype of gliomas was further examined *in vivo* by stereotactically implanting engineered glioma cells into the brains of nude mice. We used a stable miRNA sponge strategy to inhibit miR-182 *in vivo*. Compared with control tumors, intracranial tumors formed by miR-182-transduced cells displayed fewer TUNEL-positive tumor cells, higher Ki67 signals, and an increased number of CD31-positive vessels (Figure 6A). However, the number of TUNEL-positive cells markedly increased, and Ki67 and CD31 signals decreased, in miR-182-inhibited tumors (Figure 6A). Notably, the borders of miR-182-overexpressing tumors showed spike-like structures invading into the surrounding brain tissues, whereas control tumors exhibited sharp edges (Figure 6A), which indicates that miR-182 overexpression induced glioma cell invasion into the brain. Meanwhile, IHC analysis revealed that expressions of MMP-9 and VEGF-C, 2 well-known NF- $\kappa$ B targets, were upregulated in miR-182-overexpressing tumors, but attenuated in miR-182-inhibited tumors (Figure 6A). More importantly, Kaplan-Meier analysis demonstrated that mice bearing miR-182-overexpressing brain gliomas had significantly shorter survival than control animals; in contrast, mice bearing miR-182-inhibited tumors exhibited longer survival than control mice (Figure 6B). Taken together, our results suggested that miR-182-induced invasiveness and angiogenesis of glioma cells *in vivo* were largely attributable to NF- $\kappa$ B activation.

*miR-182 suppression inhibits NF- $\kappa$ B activity and malignant properties of patient-derived glioma cells (PDGCs).* We further examined the effect of miR-182 inhibition on NF- $\kappa$ B signaling in PDGCs, which more closely resemble glioma tumor cells present in the tumor mass of patients with gliomas (34). Consistent with the results described above, miR-182 was expressed at high levels in PDGCs derived from 2 independent clinical samples (Figure 7A). Inhibition of miR-182 decreased NF- $\kappa$ B-driven luciferase activity and endogenous NF- $\kappa$ B activity, but increased the luciferase activity regulated by the CYLD-3'UTR (Figure 7, B–D). TNF- $\alpha$ -induced K63-

linked poly-Ub levels of RIP1 and NEMO as well as of I $\kappa$ B $\alpha$  were also significantly attenuated in the miR-182 inhibitor-transfected PDGCs (Figure 7E). Furthermore, when compared with the control cells, PDGCs transfected with the miR-182 inhibitor exhibited markedly decreased growth (Figure 7F). Moreover, inhibition of miR-182 significantly decreased the invasiveness of PDGCs and their ability to induce tube formation of HUVECs (Figure 7, G and H). Taken together, these data suggest that suppression of miR-182 inhibited NF- $\kappa$ B activity and PDGC malignancy.

*TGF- $\beta$  induces miR-182 in gliomas.* It is notable that the coding sequence of *MIR182* is located in chromosome 7q32.1 and is also frequently amplified in clinical gliomas (35). Genomic real-time PCR analyses showed that the copy number of the *MIR182* region was increased approximately 2- to 3-fold in 35.6% of glioma samples examined (*n* = 161; data not shown). On the other hand, we recently reported that miR-182 expression was elevated in 98% of clinical glioma specimens (33), which suggests that miR-182 overexpression in gliomas is only partly due to genomic amplification. Additionally, miR-182 is induced by IL-2 in activated helper T lymphocytes (36). Interestingly, glioma cells treated with TGF- $\beta$  showed a marked increase in miR-182 expression, whereas IL-2, TNF- $\alpha$ , IL-1 $\beta$ , IL-8, IFN- $\gamma$ , and IL-6 had minimal effects on miR-182 expression (Figure 8A). In contrast, TGF- $\beta$  treatment of NHAs did not affect miR-182 expression (Supplemental Figure 3A). Concordantly, expression levels of miR-183 and miR-96, the other 2 members of the miR-183/miR-96/miR-182 cluster, was also upregulated in TGF- $\beta$ -treated glioma cells (data not shown). Importantly, the stimulatory effect of TGF- $\beta$  on miR-182 was prevented by a TGF- $\beta$  receptor I (T $\beta$ RI) inhibitor as well as by a TGF- $\beta$  neutralizing antibody (Figure 8B). Lastly, miR-182 expression was also upregulated in Smad2/Smad4-overexpressing cells and downregulated in Smad2/Smad4-silenced cells (Supplemental Figure 3, B and C). These results suggest that TGF- $\beta$  induced miR-182 expression in glioma cells.

Analysis of the *MIR182* promoter region using the CONSITE program predicted 3 typical TGF- $\beta$ -responsive elements (SREs; Figure 8C). ChIP assay showed that endogenous Smad2/Smad4 proteins bound to the first SRE in the *MIR182* promoter (Figure 8C), which indicates that the TGF- $\beta$ /Smad pathway induced miR-182 expression through directly targeting the *MIR182* promoter.

*TGF- $\beta$ -induced miR-182 contributes to sustained NF- $\kappa$ B activation.* As expected, luciferase activity of the NF- $\kappa$ B reporter significantly increased in TGF- $\beta$ -treated glioma cells, but decreased in cells treated with a T $\beta$ RI inhibitor or with a neutralizing anti-TGF- $\beta$  antibody (Figure 8D). p-IKK $\beta$  was also elevated, and expression of I $\kappa$ B $\alpha$  was reduced, in TGF- $\beta$ -treated cells (Figure 8E and Supplemental Figure 4A). Importantly, we found that K63-linked poly-Ub levels of RIP1 and NEMO and K48-linked poly-Ub level of I $\kappa$ B $\alpha$  increased in TGF- $\beta$ -treated cells (Figure 8F and Supplemental Figure 4, B–D), which indicates that TGF- $\beta$  promoted Ub conjugations of NF- $\kappa$ B signaling. Furthermore, endogenous IKK kinase activity induced by TNF- $\alpha$  was prolonged in TGF- $\beta$ -treated glioma cells (Figure 8G), which suggests that TGF- $\beta$  sustained TNF- $\alpha$ -induced NF- $\kappa$ B activation in glioma cells. However, the stimulatory effects of TGF- $\beta$  on the NF- $\kappa$ B pathway were abrogated by a miR-182 inhibitor (Figure 8, E–G, and Supplemental Figure 4, A–D). These results indicate that miR-182 was involved in TGF- $\beta$ -mediated NF- $\kappa$ B activation.

*miR-182 expression correlates with TGF- $\beta$ /Smad pathway hyperactivation and NF- $\kappa$ B activity in clinical gliomas.* Finally, we examined whether activation of the TGF- $\beta$ /Smad/miR-182/NF- $\kappa$ B axis

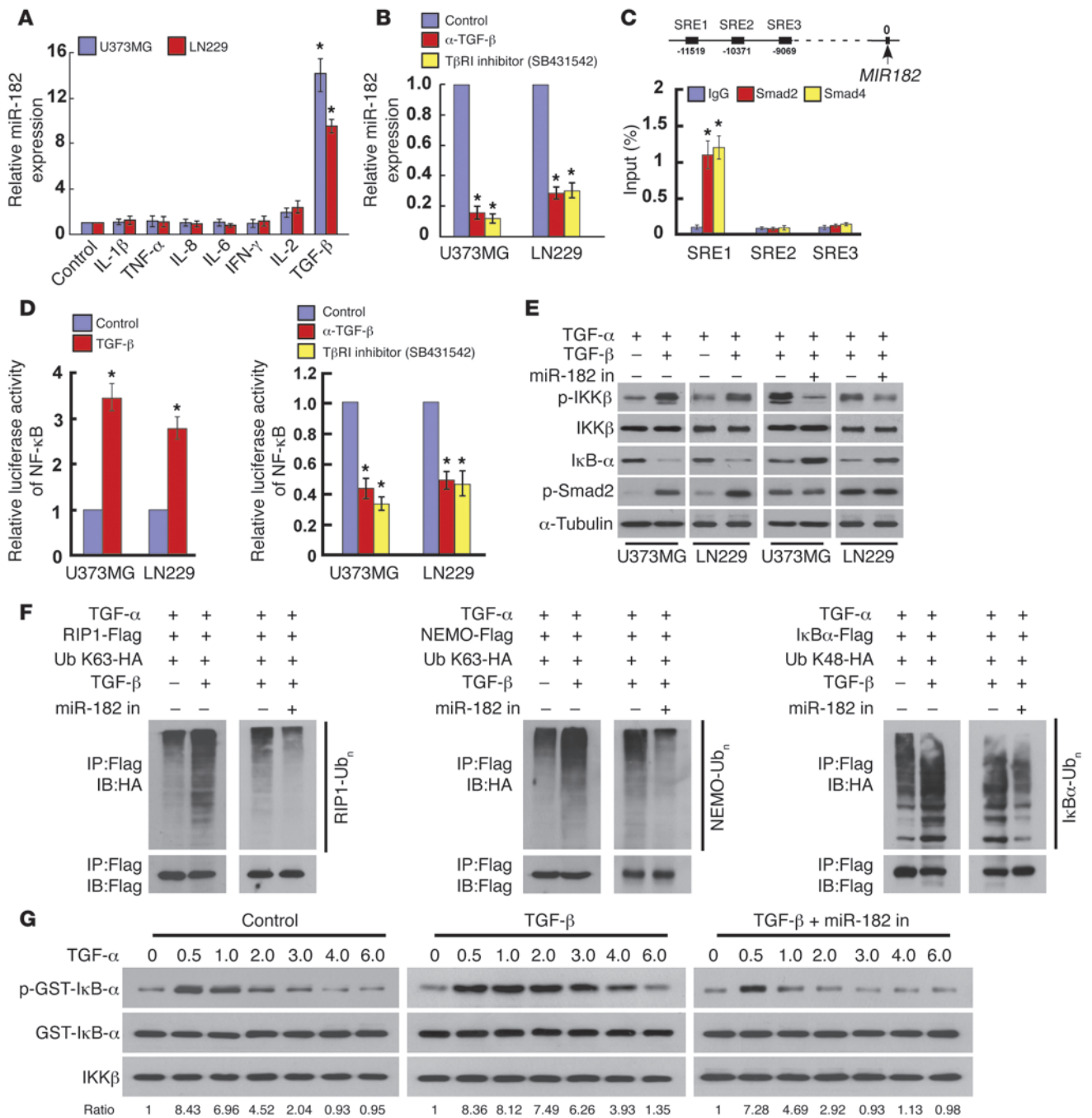


**Figure 8**

TGF- $\beta$  induces miR-182 expression. (A) Real-time PCR analysis of miR-182 expression in glioma cells treated with 10 ng/ml of the indicated cytokines or with 100 pM TGF- $\beta$  for 3 hours. Transcript levels were normalized by *U6* expression. (B) Real-time PCR analysis of miR-182 expression in indicated cells treated with or without a T $\beta$ RI inhibitor (2  $\mu$ M) or a neutralizing anti-TGF- $\beta$  antibody (2  $\mu$ g/ml) for 3 hours. (C) Schematic of typical SREs of the *MIR182* promoter. Also shown are ChIP assay results for the SREs of *MIR182* promoter physically associated with Smad2/Smad4. Expression levels of Smad2/Smad4 were analyzed by WB analysis (see Supplemental Figure 3). (D) Luciferase-reporter NF- $\kappa$ B activity in the indicated cells, either treated with TGF- $\beta$  for 3 hours or treated with or without the T $\beta$ RI inhibitor (2  $\mu$ M) or a neutralizing anti-TGF- $\beta$  antibody (2  $\mu$ g/ml) for 3 hours. (E) WB of p-IKK $\beta$ , total IKK $\beta$ , I $\kappa$ B $\alpha$ , and p-Smad2 in TNF- $\alpha$ -treated cells (10 ng/ml) in response to treatment with 100 pM TGF- $\beta$  or control. (F) WB analysis of K63-linked poly-Ub of RIP1 and NEMO and K48-linked poly-Ub of I $\kappa$ B $\alpha$  in TNF- $\alpha$ -treated cells (10 ng/ml) in response to 100 pM TGF- $\beta$ . (G) In vitro kinase assay indicated that endogenous IKK kinase activity induced by TNF- $\alpha$  was prolonged in TGF- $\beta$ -treated cells, which was abrogated by miR-182 inhibitor (see Supplemental Methods). Error bars represent mean  $\pm$  SD from 3 independent experiments. \* $P$  < 0.05.

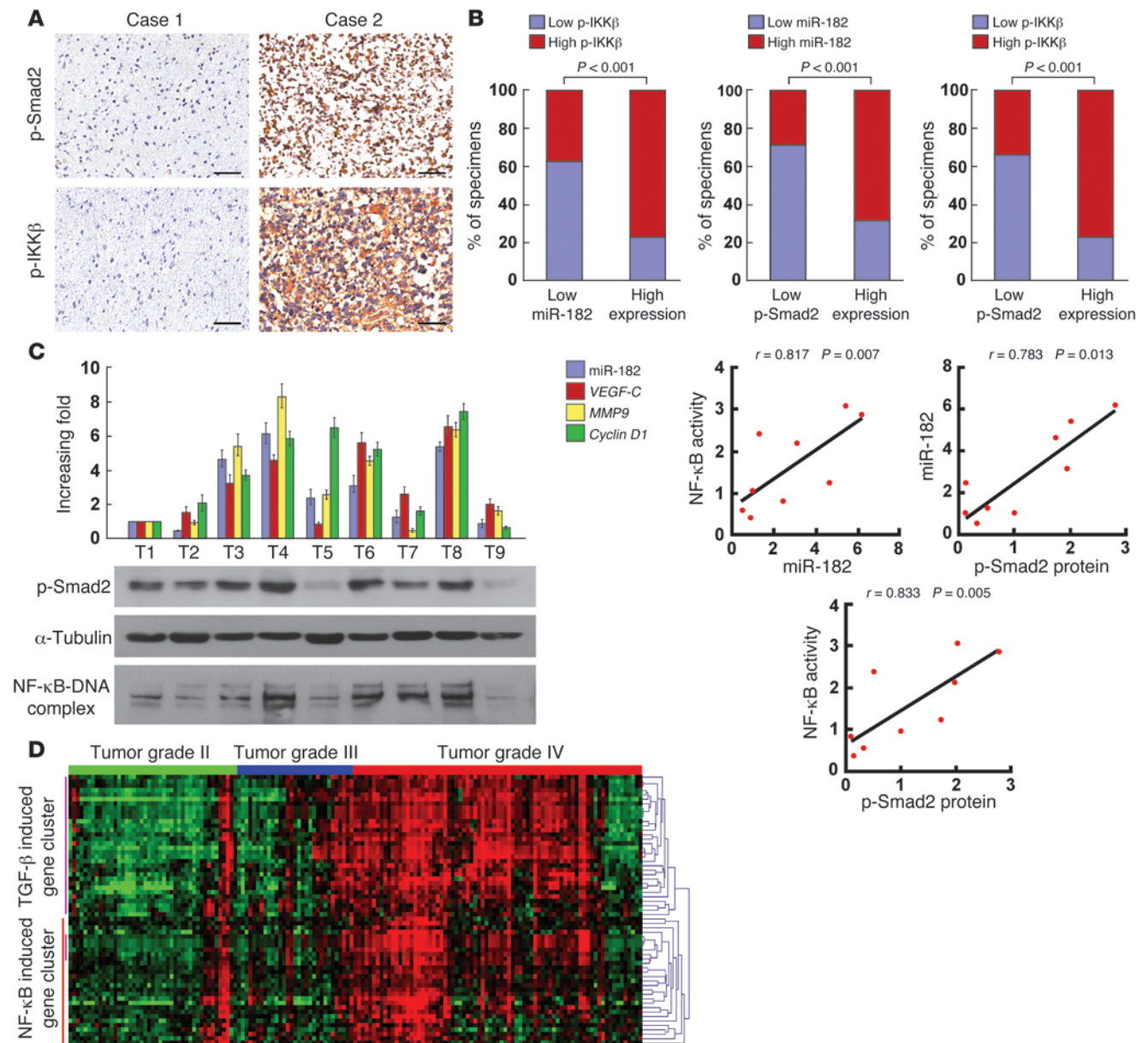


**Figure 9**

Clinical relevance of the TGF- $\beta$ /Smad/miR-182/NF- $\kappa$ B axis in human gliomas. (A) p-Smad2 levels associated with p-IKK $\beta$  (S181) expression in 161 primary human glioma specimens. 2 representative cases are shown. Scale bars: 50  $\mu$ m. (B) Percentages of samples showing low or high p-Smad2 expression in 161 primary human glioma specimens relative to the levels of p-IKK $\beta$  or miR-182. (C) Expression and correlation of miR-182 with *MMP9*, *VEGF-C*, and *Cyclin D1* mRNA expression, as well as p-Smad2 protein expression and NF- $\kappa$ B activity in 9 freshly collected human glioma samples. (D) Hierarchical clustering analysis indicated a significant correlation ( $P < 0.01$ ) between the transcriptional levels of representative TGF- $\beta$ -targeted genes (such as *SERPINE1*, *LTBP1*, and *SMAD7*) and transcriptional levels of NF- $\kappa$ B-targeted genes (such as *IL8*, *IL6*, and *NFKBIA*) in a published high-throughput microarray dataset (NCBI/GEO/GSE4290;  $n = 180$ ). Error bars represent mean  $\pm$  SD from 3 independent experiments. \* $P < 0.05$ .

identified in our glioma cell models is also evident in clinical glioma tumors. By analyzing 161 glioma tissue specimens, we found that, in agreement with a previous report (26), expression of p-Smad2, an indicator of TGF- $\beta$  activity, and miR-182 levels strongly correlated with glioma grades and, inversely, with patient survival (Supplemental Figure 5, A and B, and Supplemental Tables 4 and 5). Moreover, p-Smad2 levels were strongly associated with expression of miR-182 and p-IKK $\beta$  (S181) ( $P < 0.001$

for both; Figure 9, A and B). Consistently, miR-182 levels in 9 freshly collected clinical glioma samples positively correlated with the mRNA levels of several NF- $\kappa$ B downstream target genes, including *Cyclin D1* ( $r = 0.750$ ,  $P = 0.020$ ), *MMP9* ( $r = 0.883$ ,  $P = 0.002$ ), and *VEGF-C* ( $r = 0.700$ ,  $P = 0.036$ ), as well as NF- $\kappa$ B activity ( $r = 0.817$ ,  $P = 0.007$ ) and p-Smad2 expression ( $r = 0.787$ ,  $P = 0.013$ ) (Figure 9C). Furthermore, statistical analysis of the cohort showed that p-Smad2 was associated with significantly shorter survival of

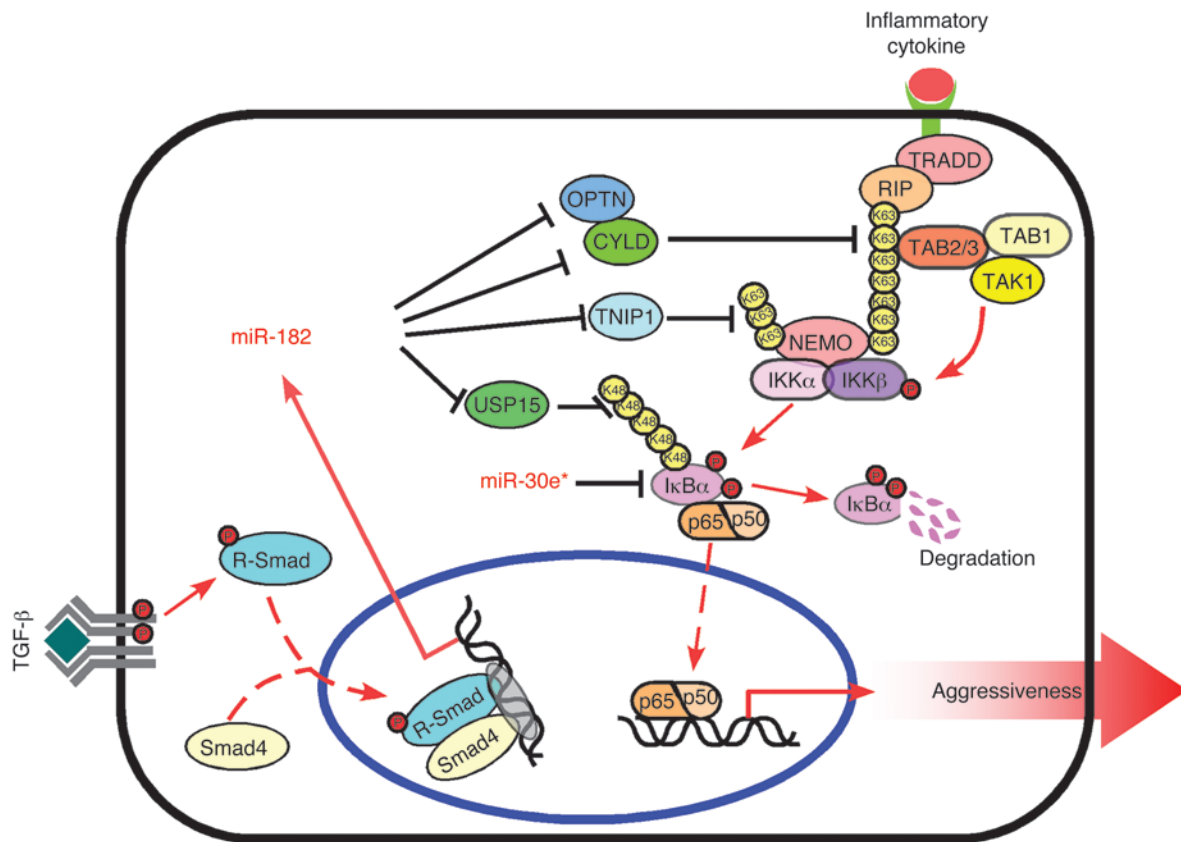


**Figure 10**  
 Hypothetical model illustrating that constitutive activation of the NF-κB pathway by miR-182 and miR-30e\* epigenetic disruption of multiple negative feedback loops leads to increased glioma progression and tumorigenesis.

patients with gliomas ( $P < 0.001$ ), which was also inversely associated with high miR-182 ( $P < 0.001$ ) and p-IKKβ ( $P < 0.001$ ) levels (Supplemental Figure 5, A–C). Additionally, analysis of a published microarray dataset (NCBI/GEO/GSE4290;  $n = 180$ ) using hierarchical clustering identified significant correlations between the transcription of classical TGF-β-induced genes (such as *SERPINE1*, *LTBP1*, and *SMAD7*) and that of NF-κB target genes (such as *IL8*, *IL6*, and *NFKBIA*) ( $P < 0.01$ ; Figure 9D). These data further support the notion that a hyperactive TGF-β/Smad pathway induces miR-182 expression, resulting in activation of NF-κB signaling and consequently leading to promotion of malignant phenotypes of gliomas and poor clinical prognosis of clinical gliomas (Figure 10).

**Discussion**

*Molecular mechanisms for CYLD regulation in gliomas.* In addition to an involvement in the development of inherited familial cylindromatosis, CYLD reduction was also found to be associated with other types of cancer, including melanoma, T cell leukemia, colon cancer, and hepatocellular carcinomas (37–39). However, the biological effect of CYLD on the development and progression of gliomas remains unclear. In our present study, results from statistical analysis of clinical specimens and an orthotopically xenografted glioma model revealed that CYLD was clinically and biologically relevant to glioma aggressiveness, further supporting the notion that CYLD functions as a tumor suppressor.

Aside from the mechanism by which mutations or deletions of *CYLD* can lead to loss of CYLD expression (40), the reduction of CYLD expression is also regulated at the transcriptional level in human cancers. For example, the transcriptional repressor Snail decreases CYLD expression in melanoma cells by directly targeting its promoter, and the Notch/Hes1 pathway sustains NF-κB activation through repression of CYLD in T cell leukemia (37, 38). CYLD can also be transcriptionally regulated through the NF-κB pathway in a negative feedback pathway (41). However, the results of our current study and published microarray analyses (NCBI/GEO/GSE4290) have shown that expression of *CYLD* mRNA is not decreased in glioma cells compared with normal brain tissues, which suggests that reduced CYLD in gliomas might be regulated via translational repression. Analyses using publicly available algorithms and the results of the present study identified CYLD as a direct target of miR-182 in gliomas. Furthermore, TGF-β/Smad induced miR-182 expression. These data suggest that TGF-β/Smad signaling is hyperactivated in high-grade gliomas, thereby increasing miR-182 expression and further reducing CYLD expression. Indeed, the hyperactivity of the TGF-β/Smad pathway correlates with glioma progression and poor prognosis of patients with malignant gliomas (26). Thus, our current study uncovers what we believe to be a novel mechanism that leads to CYLD reduction in cancer cells.

*Mechanism mediating sustained NF-κB activity in gliomas.* We recently reported that miR-30e\* is overexpressed in clinical gliomas and disrupts the NF-κB/IκBα negative feedback loop, resulting in con-



stitutively activated NF- $\kappa$ B signaling (42). In this study, we demonstrated a distinct mechanism by which miR-182 enhances the strength, and prolongs the duration, of NF- $\kappa$ B signaling through inhibition of the deubiquitination-mediated negative feedback loop. By analyzing the Cancer Genome Atlas (TCGA) database, we also found that miR-30e\* and miR-182 were not persistently coexpressed at similar levels in clinical glioblastoma multiforme (GBM) samples (Supplemental Figure 6A). However, levels of miR-182 and miR-30e\* expression were separately, and also positively, correlated with the expression of IL-8, a direct target and also an indicator of NF- $\kappa$ B activity ( $P < 0.001$  for both; Supplemental Figure 6B). This finding suggests that expression of either miR-182 or miR-30e\* could be sufficient for activation of NF- $\kappa$ B. Importantly, expression of IL-8 in GBM samples with high levels of both miR-182 and miR-30e\* was significantly higher than that in GBM tissues only showing high levels of either miRNA alone ( $P < 0.001$  for both; Supplemental Figure 6B), which suggests that miR-182 and miR-30e\* can act at least additively in stimulating the NF- $\kappa$ B signaling. Consistent with this finding, coexpression of miR-182 and miR-30e\* further potentiated NF- $\kappa$ B transcriptional activity and invasion of glioma cells compared with the effects of expressing miR-182 or miR-30e\* alone (Supplemental Figure 6, C and D). Taken together, these results suggest that miR-182 and miR-30e\* are capable of activating NF- $\kappa$ B signaling in distinct yet cooperative fashions, thereby promoting glioma tumorigenicity and invasion. The precise roles of miR-182 in NF- $\kappa$ B activation and glioma progression need to be further investigated in cells with low or no expression of miR-30e\*.

**Contribution of miR-182 to NF- $\kappa$ B signaling regulation.** It has been established that inhibition and termination of the NF- $\kappa$ B signaling cascade is tightly regulated by negative feedback mechanisms involving several NF- $\kappa$ B negative regulators, such as CYLD, A20, TNIPs, and OPTN as well as NF- $\kappa$ B inhibitor I $\kappa$ Bs (5, 6). In the present study, restoration of CYLD expression in miR-182-transduced cells only partially reversed miR-182-induced NF- $\kappa$ B activation (Supplemental Figure 7A), which suggests that other regulatory targets might also be involved. Indeed, analyses using publicly available algorithms predict that TNIP1, OPTN, and USP15 could also be potential targets of miR-182 (Supplemental Figure 7B). We found that the expression levels of, and the reporter activity driven by, the 3'UTR of TNIP1, OPTN, or USP15 could be drastically repressed in miR-182-transduced cells, but increased in miR-182-inhibited cells, and that miR-182 was selectively associated with *TNIP1*, *OPTN*, and *USP15* (Supplemental Figure 7, C-E). These results suggest that miR-182 could directly regulate these transcripts. Thus, the identification of the multitarget function of miR-182 may reveal a novel mechanism by which the negative feedback loops for regulating NF- $\kappa$ B signaling are abrogated in cancer cells (Figure 10). Moreover, these results also suggest that the aforementioned miR-182-regulated targets might be also involved in glioma progression, which is currently being investigated in our laboratory.

Interestingly, A20 has been found to be overexpressed in clinical gliomas, and overexpression of A20 establishes resistance to TNF- $\alpha$ - or TRAIL-induced apoptosis in glioblastoma (43, 44). On the other hand, however, A20 does not exhibit any significant preference in deubiquitinating K63-linked poly-Ub chains in vitro (45, 46), which suggests that A20 might cooperate with other proteins to inhibit NF- $\kappa$ B signaling. It has previously been demonstrated that TNIP1, an A20-binding inhibitor of

NF- $\kappa$ B, physically interacts with A20 and functions as an adaptor for recruitment of A20 to its target, NEMO, and that silencing TNIP1 prevents deubiquitylation of NEMO by A20 (47, 48). Whether the inhibitory effect of overexpressed A20 on NF- $\kappa$ B signaling in gliomas can be attenuated by miR-182-mediated TNIP1 repression requires further investigation.

**Effect of miR-182 on TGF- $\beta$ /Smad-induced NF- $\kappa$ B activation.** TGF- $\beta$  and inflammatory cytokines, such as IL-1 $\beta$  and TNF- $\alpha$ , are mutual inhibitors of each other, especially in regulating NF- $\kappa$ B signaling. For instance, TGF- $\beta$  can induce expression of I $\kappa$ B $\alpha$  that inhibits NF- $\kappa$ B signaling (49, 50). TGF- $\beta$ /Smad-induced Smad7 prevents formation of the TRAF2/TAK1/TAB2/TAB3 complex and disrupts the IRAK4/IRAK1/Pellino1/TRAF6 complex, resulting in inhibition of TNF- $\alpha$ - or IL-1 $\beta$ -stimulated NF- $\kappa$ B activation (51, 52). TRAF2/TRAF6-mediated K63-linked polyubiquitination of TAK1, which can be deubiquitinated by CYLD, is required for activation of TAK1 (53). Here we showed that miR-182 directly repressed USP15, the Ub-specific protease that prevents I $\kappa$ B $\alpha$  proteasomal degradation through removal of K48-linked Ub chains (54). Interestingly, we also found that Smad7 expression was decreased in miR-182-transduced cells, but increased in miR-182-inhibited cells (Supplemental Figure 8, A-C). Thus, it is plausible that miR-182 modulates TGF- $\beta$ -mediated NF- $\kappa$ B activation through multiple mechanisms, namely by downregulating USP15 to promote I $\kappa$ B $\alpha$  proteasomal degradation, reducing CYLD to activate TAK1, and decreasing Smad7 to enhance the formation of the TRAF2/TAK1/TAB2/TAB3 complex or the IRAK4/IRAK1/Pellino1/TRAF6 complex. Interestingly, USP15 was recently reported to play a role in the activation of TGF- $\beta$  signaling (55). On the other hand, analysis of the TCGA datasets indicated that *USP15* is expressed at various levels among 4 clinical relevant subtypes of GBM samples (data not shown). These observations warrant further investigation of the effect of miR-182 on the TGF- $\beta$  pathway in gliomas.

**Therapeutic and prognostic value of miR-182.** Upregulation of miR-182 has been previously reported in epithelial ovarian cancer and melanoma (56, 57). Importantly, overexpressing miR-182 in epithelial ovarian cancer cells significantly promotes tumor growth and enhances the metastatic potential of melanoma cells in vivo, implicating miR-182 as an oncomir (56, 57). miR-182 overexpression in breast tumor cells leads to genomic instability through reducing BRCA1 protein and renders cells hypersensitive to PARP1 inhibitors, which suggests that miR-182 expression may affect therapeutic responses (58). We recently reported that increased miR-182 expression significantly correlates with glioma WHO tumor grades (33). In light of these separate prior studies, our present results suggest that miR-182 could be a new and independent prognostic indicator for evaluating the clinical outcomes of cancer patients.

Despite therapeutic advancements, current treatments against malignant gliomas remain challenging due to ineffective targeting of infiltrating glioma cells and formation of abnormal, dysfunctional tumor vasculature (24, 59, 60). The TGF- $\beta$ /Smad pathway has been considered as a therapeutic target for gliomas (61, 62). In this context, however, given the opposing roles of the TGF- $\beta$ /Smad pathway in glioma progression, to distinguish its tumor-suppressive role from the tumor-promoting potential in clinical gliomas represents a challenge. Here, we demonstrated that miR-182 was significantly upregulated in glioma cells treated with TGF- $\beta$ , which functionally promoted the aggressiveness of gliomas both in vitro and in vivo. Notably, TGF- $\beta$  treatment did not induce miR-182 in NHAs. Therefore, understanding the precise regula-



tory mechanism of miR-182 in glioma progression will not only advance our knowledge of the pathogenesis of gliomas, but also permit the development of novel therapeutic strategies and to identify an effective biomarker to predict outcomes for patients with malignant gliomas.

## Methods

**Cell lines and primary cultured tumor cells.** Primary NHAs were purchased from Sciencell Research Laboratories and cultured according to the manufacturer's instructions. Glioma cell lines LN382T, A172, T98G, LN18, LN229, LN464, SNB19, U373MG, U87MG, LN444, LN443, LN428, U118MG, LN-Z308, and LN319 were from ATCC, E. Van Meir (Emory University, Atlanta, Georgia, USA), or Y.-H. Zhou (University of California, Irvine, California, USA). These cells were grown in DMEM supplemented with 10% FBS. Fresh brain tumor tissues, obtained from the First Affiliated Hospital of Sun Yat-sen University, were collected and processed within 30 minutes after resection. The primary cultured tumor cells were obtained after mechanical dissociation, as previously described (34).

**Plasmids, virus production, and infection of target cells.** The human *MIR182* gene was PCR amplified from genomic DNA and cloned into a pMSCV-puro retroviral vector. miR-182 sponge was constructed by annealing, purifying, and cloning oligonucleotides containing 6 tandem "bulged" miR-182 binding motifs into the pMSCV vector. Human *CYLD*, *TNIP1*, *OPTN*, and *USP15* were amplified by PCR from a human liver cDNA library (Clontech) and cloned into the pMSCV vector. The 3'UTR region of human *CYLD*, *TNIP1*, *OPTN*, and *USP15* genes, generated by PCR amplification from NHAs, were cloned into the *SacI/XmaI* sites of pGL3 luciferase reporter plasmid (Promega) and pEGFP-C3 vector (Clontech). pBabe-Puro-IκBα-mut (plasmid 15291) expressing mutant IκBα was from Addgene. pNF-κB-luc and control plasmids (Clontech) were used to determine NF-κB activity. Transfection of siRNAs or plasmids was performed using the Lipofectamine 2000 reagent (Invitrogen) according to the manufacturer's instructions. Stable cell lines expressing miR-182 and miR-182 sponge were generated via retroviral infection using HEK293T cells as previously described (63) and selected with 0.5 μg/ml puromycin for 10 days.

**Tissue specimens and patient information.** A total of 161 paraffin-embedded, archived clinical glioma specimens, including WHO I-IV grade tumors and 14 freshly snap-frozen glioma tissues, were histopathologically diagnosed at the First Affiliated Hospital of Sun Yat-sen University from 2000 to 2010. Normal brain tissues were obtained from individuals who died in traffic accidents and confirmed to be free of any preexisting pathologically detectable conditions. Prior donor consent and approval from the Institutional Research Ethics Committee were obtained.

**RNA extraction and real-time quantitative PCR.** Total miRNA from cultured cells and fresh surgical glioma tissues was extracted using the mirVana miRNA Isolation Kit (Ambion) according to the manufacturer's instructions. cDNA was synthesized using the Taqman miRNA reverse transcription kit (Applied Biosystems), and the expression level of miR-182 was quantified using miRNA-specific TaqMan MiRNA Assay Kit (Applied Biosystems). Real-time PCR was performed using the Applied Biosystems 7500 Sequence Detection system. The expression of miRNA was defined based on Ct, and relative expression levels were calculated as  $2^{-(Ct_{miR-182} - Ct_{U6})}$  after normalization with reference to the quantification of *U6* small nuclear RNA expression.

**Western blotting analysis (WB).** WB was performed as previously described (63) using the following antibodies: anti-CYLD, anti-TNIP1, and anti-OPTN (Sigma-Aldrich); anti-IκBα, anti-p-IκBα, anti-p-IKKβ, anti-Smad2, and anti-Smad4 (Cell Signaling); anti-IKKβ (Santa Cruz Biotechnology); and anti-USP15 (Abcam). To control sample loading, the blotting membranes were stripped and reprobed with an anti-α-tubulin antibody (Sigma-Aldrich).

**IHC.** IHC analysis was performed in 161 clinical glioma tissue sections as previously described (63). IHC stained tumor sections were examined and scored independently by 2 observers for positively stained tumor cells and IHC signal intensity. The proportion of tumor cells was scored as follows: 0, no positive tumor cells; 1, <10% positive tumor cells; 2, 10%–50% positive tumor cells; 3, >50% positive tumor cells. The intensity of staining was graded according to the following criteria: 0, no staining; 1, weak staining (light yellow); 2, moderate staining (yellow-brown); 3, strong staining (brown). The staining index (SI) was calculated as the product of staining intensity score and proportion of positive tumor cells. We assessed the indicated protein expression in IHC-stained tumor sections determined by SI scores as 0, 1, 2, 3, 4, 6, and 9. Cutoff values were chosen on the basis of a measure of heterogeneity using the log-rank test with respect to overall survival.

**Luciferase assay.** 3,000 cells were seeded in triplicate in 48-well plates and allowed to settle for 24 hours. 100 ng luciferase reporter plasmids or the control luciferase plasmid plus 1 ng pRL-TK renilla plasmid (Promega) were transfected into glioma cells using the Lipofectamine 2000 reagent (Invitrogen). Luciferase and renilla signals were determined 24 hours after transfection using a Dual Luciferase Reporter Assay Kit (Promega).

**miRNP IP assay.** Cells were cotransfected with a plasmid that encodes HA-Ago1 and miR-182 (100 nM), followed by HA-Ago1 IP using an anti-HA antibody. Real-time PCR analysis of the IP material was used to test the association of the mRNA of *CYLD*, *TNIP1*, *OPTN*, *USP15*, *FOXO3a*, and *GAPDH* with the RISC complex.

**EMSA.** EMSA was performed using the LightShift Chemiluminescent EMSA kit (Pierce Biotechnology). The following DNA probes containing specific binding sites were used: NF-κB sense, 5'-AGTTGAGGGGACTTTCCAG-GC-3'; NF-κB antisense, 5'-GCCTGGGAAAGTCCCCTCAAC-3'; OCT-1 sense, 5'-TGTCGAATGCAAATCACTAGAA-3'; OCT-1 antisense, 5'-TTC-TAGTGATTTGCATTCGACA-3'.

**Cell invasion assay.** Various glioma cells ( $2 \times 10^4$ ) were plated on the top side of a polycarbonate Transwell filter (with Matrigel) in the upper chamber of the BioCoat Invasion Chambers (BD) and incubated at 37°C for 22 hours, followed by removal of cells inside the upper chamber with cotton swabs. Migrated and invaded cells on the lower membrane surface were fixed in 1% paraformaldehyde, stained with hematoxylin, and counted under a microscope (10 random fields per well,  $\times 100$  magnification). Cell counts were expressed as the mean number of cells per field.

**ChIP.**  $2 \times 10^6$  cells in a 100-mm culture dish were treated with 1% formaldehyde to cross-link proteins to DNA. The cell lysates were sonicated to shear DNA to sizes of 300–1,000 bp. Equal aliquots of chromatin supernatants were separated and incubated with 1 μg anti-Smad2 and anti-Smad4 antibodies (Cell Signaling) or an anti-IgG antibody (negative control; Millipore) overnight at 4°C with rotation. After reverse cross-link of protein/DNA complexes to free DNA, PCR was performed using specific primers.

**Intracranial brain tumor xenografts, IHC, and H&E staining.** Various glioma cells ( $5 \times 10^5$ ) were stereotactically implanted into the brains of individual mice ( $n = 5$  per group). Mice were monitored daily and euthanized when moribund. Whole brains were removed, paraffin embedded, sectioned to 4-μm-thick slides, and stained with H&E or separately with anti-Ki67 (Dako), anti-MMP-9 (Cell Signaling), anti-VEGF-C (Cell Signaling), or anti-CD31 (Dako) antibodies. Images were captured using the AxioVision Rel.4.6 computerized image analysis system (Carl Zeiss). Proliferation index was quantified by counting the proportion of Ki67-positive cells. The apoptotic index was measured as percent TUNEL-positive cells.

**Microarray data processing and visualization.** Microarray hybridization, data generation, and normalization were performed at Shanghai Biochip Corp. following standard Agilent protocols. Bioinformatic analysis and visualization of microarray data were performed using MeV 4.6 (<http://www.tm4.org/mev/>).



**Accession numbers.** The microarray data described herein have been deposited in the National Center for Biotechnology Information Gene Expression Omnibus (<http://www.ncbi.nlm.nih.gov/geo/>) under accession no. GSE33293.

**Statistics.** All statistical analyses were carried out using the SPSS 10.0 statistical software package. The  $\chi^2$  test was used to analyze the relationship between CYLD expression and clinicopathological characteristics. Bivariate correlations between study variables were calculated by Spearman's rank correlation coefficients. A *P* value less than 0.05 was considered statistically significant.

**Study approval.** The use of human glioma tissue specimens was evaluated and approved by the Ethical Committee of the First Affiliated Hospital of Sun Yat-sen University, and written informed consent was obtained from all participants or their appropriate surrogates. All animal studies were conducted with the approval of the Sun Yat-sen University Institutional Animal Care and Use Committee and were performed in accordance with established guidelines.

## Acknowledgments

This work was supported by the GDUPS (2012) and Natural Science Foundation of China (grant nos. 81071780, 81030048, 81071647, 81071762, 81272196, and 81272198); The Science and Technology Department of Guangdong Province (grant no. S2011020002757).

Received for publication December 8, 2011, and accepted in revised form July 26, 2012.

Address correspondence to: Jun Li, Zhongshan School of Medicine, Sun Yat-sen University, 74 Zhongshan Road II, Guangzhou, Guangdong, 510080, China. Phone: 86.20.87335828; Fax: 86.20.87335828; E-mail: lijun37@mail.sysu.edu.cn.

- Pikarsky E, et al. NF-kappaB functions as a tumour promoter in inflammation-associated cancer. *Nature*. 2004;431(7007):461–466.
- Karin M, Greten FR. NF-kappaB: linking inflammation and immunity to cancer development and progression. *Nat Rev Immunol*. 2005;5(10):749–759.
- Karin M. Nuclear factor-kappaB in cancer development and progression. *Nature*. 2006;441(7092):431–436.
- Hayden MS, Ghosh S. Shared principles in NF-kappaB signaling. *Cell*. 2008;132(3):344–362.
- Wertz IE, Dixit VM. Signaling to NF-kappaB: regulation by ubiquitination. *Cold Spring Harb Perspect Biol*. 2010;2(3):a003350.
- Liu S, Chen ZJ. Expanding role of ubiquitination in NF-kappaB signaling. *Cell Res*. 2011;21(1):6–21.
- Ea CK, Deng L, Xia ZP, Pineda G, Chen ZJ. Activation of IKK by TNFalpha requires site-specific ubiquitination of RIP1 and polyubiquitin binding by NEMO. *Mol Cell*. 2006;22(2):245–257.
- Wang C, et al. TAK1 is a ubiquitin-dependent kinase of MKK and IKK. *Nature*. 2001;412(6844):346–351.
- Deng L, et al. Activation of the IkkappaB kinase complex by TRAF6 requires a dimeric ubiquitin-conjugating enzyme complex and a unique polyubiquitin chain. *Cell*. 2000;103(2):351–361.
- Ghosh S, Baltimore D. Activation in vitro of NF-kappa B by phosphorylation of its inhibitor I kappa B. *Nature*. 1990;344(6267):678–682.
- Chen ZJ, Parent L, Maniatis T. Site-specific phosphorylation of IkkappaBalpha by a novel ubiquitination-dependent protein kinase activity. *Cell*. 1996;84(6):853–862.
- Tokunaga F, et al. Involvement of linear polyubiquitination of NEMO in NF-kappaB activation. *Nat Cell Biol*. 2009;11(2):123–132.
- Xia ZP, et al. Direct activation of protein kinases by unanchored polyubiquitin chains. *Nature*. 2009;461(7260):114–119.
- Duwel M, Hadian K, Krappmann D. Ubiquitin conjugation and deconjugation in NF-kappaB signaling. *Subcell Biochem*. 2010;54:88–99.
- Lee EG, et al. Failure to regulate TNF-induced NF-kappaB and cell death responses in A20-deficient mice. *Science*. 2000;289(5488):2350–2354.
- Kovalenko A, et al. The tumour suppressor CYLD negatively regulates NF-kappaB signalling by deubiquitination. *Nature*. 2003;424(6950):801–805.
- Trompouki E, et al. CYLD is a deubiquitinating enzyme that negatively regulates NF-kappaB activation by TNFR family members. *Nature*. 2003;424(6950):793–796.
- Sun SC. CYLD: a tumor suppressor deubiquitinase regulating NF-kappaB activation and diverse biological processes. *Cell Death Differ*. 2010;17(1):25–34.
- Wertz IE, et al. De-ubiquitination and ubiquitin ligase domains of A20 downregulate NF-kappaB signalling. *Nature*. 2004;430(7000):694–699.
- Evans PC, et al. Zinc-finger protein A20, a regulator of inflammation and cell survival, has de-ubiquitinating activity. *Biochem J*. 2004;378(pt 3):727–734.
- Hymowitz SG, Wertz IE. A20: from ubiquitin editing to tumour suppression. *Nat Rev Cancer*. 2010;10(5):332–341.
- Huang L, et al. ABINs inhibit EGF receptor-mediated NF-kappaB activation and growth of EGF receptor-overexpressing tumour cells. *Oncogene*. 2008;27(47):6131–6140.
- Zhu G, Wu CJ, Zhao Y, Ashwell JD. Optineurin negatively regulates TNFalpha-induced NF-kappaB activation by competing with NEMO for ubiquitinated RIP. *Curr Biol*. 2007;17(16):1438–1443.
- Furnari FB, et al. Malignant astrocytic glioma: genetics, biology, and paths to treatment. *Genes Dev*. 2007;21(21):2683–2710.
- Seoane J, Le HV, Shen L, Anderson SA, Massague J. Integration of Smad and forkhead pathways in the control of neuroepithelial and glioblastoma cell proliferation. *Cell*. 2004;117(2):211–223.
- Bruna A, et al. High TGFbeta-Smad activity confers poor prognosis in glioma patients and promotes cell proliferation depending on the methylation of the PDGF-B gene. *Cancer Cell*. 2007;11(2):147–160.
- Ikushima H, et al. Autocrine TGF-beta signaling maintains tumorigenicity of glioma-initiating cells through Sry-related HMG-box factors. *Cell Stem Cell*. 2009;5(5):504–514.
- Penuelas S, et al. TGF-beta increases glioma-initiating cell self-renewal through the induction of LIF in human glioblastoma. *Cancer Cell*. 2009;15(4):315–327.
- Park JI, et al. Transforming growth factor-beta1 activates interleukin-6 expression in prostate cancer cells through the synergistic collaboration of the Smad2, p38-NF-kappaB, JNK, and Ras signaling pathways. *Oncogene*. 2003;22(28):4314–4332.
- Neil JR, Schiemann WP. Altered TAB1: kappaB kinase interaction promotes transforming growth factor beta-mediated nuclear factor-kappaB activation during breast cancer progression. *Cancer Res*. 2008;68(5):1462–1470.
- Valastyan S, et al. A pleiotropically acting microRNA, miR-31, inhibits breast cancer metastasis. *Cell*. 2009;137(6):1032–1046.
- Subramanyam D, et al. Multiple targets of miR-302 and miR-372 promote reprogramming of human fibroblasts to induced pluripotent stem cells. *Nat Biotechnol*. 2011;29(5):443–448.
- Jiang L, et al. miR-182 as a prognostic marker for glioma progression and patient survival. *Am J Pathol*. 2010;177(1):29–38.
- Lee J, et al. Tumor stem cells derived from glioblastomas cultured in bFGF and EGF more closely mirror the phenotype and genotype of primary tumors than do serum-cultured cell lines. *Cancer Cell*. 2006;9(5):391–403.
- Schrock E, et al. Comparative genomic hybridization of human malignant gliomas reveals multiple amplification sites and nonrandom chromosomal gains and losses. *Am J Pathol*. 1994;144(6):1203–1218.
- Stittich AB, et al. The microRNA miR-182 is induced by IL-2 and promotes clonal expansion of activated helper T lymphocytes. *Nat Immunol*. 2010;11(11):1057–1062.
- Massoumi R, et al. Down-regulation of CYLD expression by Snail promotes tumor progression in malignant melanoma. *J Exp Med*. 2009;206(1):221–232.
- Espinosa L, et al. The Notch/Hes1 pathway sustains NF-kappaB activation through CYLD repression in T cell leukemia. *Cancer Cell*. 2010;18(3):268–281.
- Hellerbrand C, et al. Reduced expression of CYLD in human colon and hepatocellular carcinomas. *Carcinogenesis*. 2007;28(1):21–27.
- Bignell GR, et al. Identification of the familial cyclinomatosis tumour-suppressor gene. *Nat Genet*. 2000;25(2):160–165.
- Jono H, et al. NF-kappaB is essential for induction of CYLD, the negative regulator of NF-kappaB: evidence for a novel inducible autoregulatory feedback pathway. *J Biol Chem*. 2004;279(35):36171–36174.
- Jiang L, et al. MicroRNA-30e\* promotes human glioma cell invasiveness in an orthotopic xenotransplantation model by disrupting the NF-kappaB/IkappaBalpha negative feedback loop. *J Clin Invest*. 2012;122(1):33–47.
- Hjelmeland AB, et al. Targeting A20 decreases glioma stem cell survival and tumor growth. *PLoS Biol*. 2010;8(2):e1000319.
- Bellail AC, Olson JJ, Yang X, Chen ZJ, Hao C. A20 ubiquitin ligase-mediated polyubiquitination of RIP1 inhibits caspase-8 cleavage and TRAIL-induced apoptosis in glioblastoma. *Cancer Discov*. 2012;2(2):140–155.
- Komander D, Barford D. Structure of the A20 OTU domain and mechanistic insights into deubiquitination. *Biochem J*. 2008;409(1):77–85.
- Lin SC, et al. Molecular basis for the unique deubiquitinating activity of the NF-kappaB inhibitor A20. *J Mol Biol*. 2008;376(2):526–540.
- Mauro C, et al. ABIN-1 binds to NEMO/IKK-gamma and co-operates with A20 in inhibiting NF-kB. *J Biol Chem*. 2006;281(27):18482–18488.
- Heyninck K, Kreike MM, Beyaert R. Structure-function analysis of the A20-binding inhibitor of NF-kappa B activation, ABIN-1. *FEBS Lett*. 2003;536(1–3):135–140.
- Ghafoori P, Yoshimura T, Turpie B, Masli S. Increased IkappaB alpha expression is essential for the tolerogenic property of TGF-beta-exposed APCs. *FASEB J*. 2009;23(7):2226–2234.
- Arsura M, Wu M, Sonenshein GE. TGF beta 1 inhibits NF-kappa B/Rel activity inducing apoptosis of B cells: transcriptional activation of I kappa B alpha. *Immunity*. 1996;5(1):31–40.
- Hong S, et al. Smad7 binds to the adaptors TAB2 and TAB3 to block recruitment of the kinase TAK1 to the



- adaptor TRAF2. *Nat Immunol.* 2007;8(5):504–513.
52. Lee YS, et al. Smad7 and Smad6 bind to discrete regions of Pellino-1 via their MH2 domains to mediate TGF-beta1-induced negative regulation of IL-1R/TLR signaling. *Biochem Biophys Res Commun.* 2010;393(4):836–843.
53. Sorrentino A, et al. The type I TGF-beta receptor engages TRAF6 to activate TAK1 in a receptor kinase-independent manner. *Nat Cell Biol.* 2008;10(10):1199–1207.
54. Schweitzer K, Bozko PM, Dubiel W, Naumann M. CSN controls NF-kappaB by deubiquitinylation of I kappa B alpha. *EMBO J.* 2007;26(6):1532–1541.
55. Eichhorn PJ, et al. USP15 stabilizes TGF-beta receptor I and promotes oncogenesis through the activation of TGF-beta signaling in glioblastoma. *Nat Med.* 2012;18(3):429–435.
56. Zhang L, et al. Genomic and epigenetic alterations deregulate microRNA expression in human epithelial ovarian cancer. *Proc Natl Acad Sci U S A.* 2008;105(19):7004–7009.
57. Segura MF, et al. Aberrant miR-182 expression promotes melanoma metastasis by repressing FOXO3 and microphthalmia-associated transcription factor. *Proc Natl Acad Sci U S A.* 2009;106(6):1814–1819.
58. Moskwa P, et al. miR-182-mediated downregulation of BRCA1 impacts DNA repair and sensitivity to PARP inhibitors. *Mol Cell.* 2011;41(2):210–220.
59. Holland EC. Gliomagenesis: genetic alterations and mouse models. *Nat Rev Genet.* 2001;2(2):120–129.
60. Zhu Y, Parada LF. The molecular and genetic basis of neurological tumours. *Nat Rev Cancer.* 2002;2(8):616–626.
61. Seoane J. The TGFbeta pathway as a therapeutic target in cancer. *Clin Transl Oncol.* 2008;10(1):14–19.
62. Yingling JM, Blanchard KL, Sawyer JS. Development of TGF-beta signalling inhibitors for cancer therapy. *Nat Rev Drug Discov.* 2004;3(12):1011–1022.
63. Li J, et al. Astrocyte elevated gene-1 is a novel prognostic marker for breast cancer progression and overall patient survival. *Clin Cancer Res.* 2008;14(11):3319–3326.